INSTITUTE OF PHYSICS PUBLISHING WAVES IN RANDOM MEDIA

Waves Random Media **13** (2003) 339–354 PII: S0959-7174(03)62458-4

Microwave sea return at moderate to high incidence angles

William J Plant

Applied Physics Laboratory, University of Washington, Seattle, WA 98105-6698, USA

Received 22 April 2003, in final form 11 July 2003
Published 18 September 2003
Online at stacks.iop.org/WRM/13/339

Abstract

Bragg scattering is widely recognized as the dominant mechanism by which the ocean surface backscatters microwave radiation, but efforts to identify other, non-Bragg sources of this scattering have been pursued for many years. Non-Bragg backscattering from the sea surface is known to occur at incidence angles close to 0° and 90°. In this paper Bragg scattering is shown to explain most features of sea surface backscatter for incidence angles between about 20° and 80°, except when it predicts very small mean cross sections. The often-quoted evidence for non-Bragg scattering in this incidence angle range is that σ_o(HH) is occasionally found to be larger than or equal to σ_o(VV) for short integration times. We show that because of fading this is not evidence of non-Bragg scattering. For incidence angles up to about 50°, standard Bragg/composite surface scattering theory yields probabilities of finding $\sigma_o(\mathrm{HH}) > \sigma_o(\mathrm{VV})$ that are only slightly smaller than those found experimentally. As the incidence angle increases, greater differences between theoretical and experimental probabilities are found. The addition of Bragg scattering from bound, tilted waves brings theory into excellent agreement with experiment at incidence angles near 45° but still cannot account adequately for the probability of $\sigma_o(\mathrm{HH}) > \sigma_o(\mathrm{VV})$ or observed σ_o(HH) cross sections at higher incidence angles. We show that the addition of a small, non-Bragg cross section that is independent of the incidence angle and polarization, brings simulated cross sections and probability distributions into good agreement with data. A possible source of this small, non-Bragg sea return is sea spray just above the air/sea interface.

1. Bragg and non-Bragg scattering

Bragg backscattering from rough water surfaces is a resonant mechanism in which backscatter is due to a particular, Bragg-resonant surface wave. The intensity of Bragg backscatter is proportional to the spectral density of this 'Bragg wave' and the Doppler shift induced in the return signal is equal to its frequency, changing signs for advancing and receding waves.

0959-7174/03/040339+16$30.00

The conditions that must be satisfied for Bragg backscattering to occur are that surface slopes not be too large, that the vertical component of the wavenumber of the incident radiation be small compared to surface displacement, that no multiple scattering occurs from the surface and that the incident radiation illuminates all parts of the surface. When applied to the sea surface, the first of these conditions is usually satisfied but the second is not (Plant 1990). The third and fourth conditions limit the applicability to incidence angles not too close to 90°. Composite surface theory was developed to handle the second condition (Wright 1968, Bass *et al* 1968). The sea surface is imagined to be composed of small facets over which long surface waves are essentially flat while the smaller ones satisfy the second condition. This idea cannot be applied to incidence angles very near zero because the Bragg wave becomes too long and high in this region. Plant has recently shown that this limitation can be overcome with a slightly expanded version of the theory that uses the full Kirchoff integral, to which Bragg scattering is an approximation (Plant 2002). The fraction of backscatter that can be approximated as Bragg increases with increasing incidence angle at low angles and decreases with increasing wind speed. Since its introduction, standard Bragg/composite surface theory has been known to account better for normalized radar cross sections of the sea, σ_o, at high incidence angles when vertical polarization is used for both transmit and receive signals (VV) than when horizontal polarization (HH) is used (Wright 1968). Predicted cross sections at HH, σ_o (HH), are too small at high incidence angles. Plant recently proposed that bound, tilted short waves produced by longer waves exist on the sea surface and that scattering from these bound waves can account for anomalies in Doppler spectra and for part of the under-prediction of σ_o(HH) (Plant 1997). Nevertheless, the prediction of σ_o(HH) at high incidence angles by Bragg/composite surface scattering theory has remained too low.

Because of this under-prediction, and because of the approximate nature of Bragg/composite surface scattering theory, attempts have been made over the years to add non-Bragg scattering from the sea surface to the theory (Lyzenga *et al* 1983, Donelan and Pierson 1987, Lee *et al* 1999, Walker 2000). Evidence in addition to the under-prediction of σ_o(HH) that has sustained this search has been the observation of occasions when HH backscatter is greater than VV, either in cross sections averaged over short times or in Doppler spectra obtained in short times (Kwoh *et al* 1988, Lee *et al* 1995, 1997, 1999, Rufatt 1999). This has been considered evidence of non-Bragg scattering because Bragg/composite surface theory predicts that $\langle\sigma_o(\mathrm{VV})\rangle$ is greater than $\langle\sigma_o(\mathrm{HH})\rangle$, where $\langle\ \rangle$ indicates the mean value. These mean cross sections, however, are those that have been obtained with very long averaging times. The assumption is that phase decorrelation between fields backscattered from different facets causes products of these fields to average to zero so that total cross section, which is proportional to the square of the fields, can be obtained by averaging cross sections from all facets. For short integration times, though, the products of fields from different facets that result from squaring do not average to zero. That is, fading occurs. Due to fading, Bragg scattering theory can yield $\sigma_o(\mathrm{HH}) > \sigma_o(\mathrm{VV})$ for short integration times.

In section 2, we describe the experimental conditions and data obtained with very short integration times during Phase II of the SAXON-FPN experiment in 1991. We compare these data with predictions of the standard Bragg/composite surface scattering theory in section 3. We find that near 45° incidence angles, the agreement is rather good but that it deteriorates at higher incidence angles. In section 4, we add bound, tilted waves to the scattering model and show that this improves the agreement but that a substantial under-prediction of σ_o(HH) at high incidence angles still occurs. In section 5, we show that the under-prediction can be corrected by postulating a small additional cross section that is independent of incidence angle and polarization. One possibility for the origin of this small, non-Bragg sea return is spray near the surface. We show that reasonable scenarios for droplet populations in sea spray near

the surface can yield an additional cross section of the right magnitude that is independent of incidence angle and polarization. Finally, in section 6, we conclude that non-Bragg scattering plays little role in microwave sea return in the incidence angle range from 20° to 80°, except when the mean Bragg cross section is very small.

2. Description of data and experiment

The data used here were collected between December 10 and 15, 1991, during Phase II of the SAXON-FPN experiment conducted by the Office of Naval Research (Plant and Alpers 1994). Two coherent, CW microwave systems with pencil-beam antennas were operated from the German Research Platform 'NORDSEE' (Forschungs Plattform NORDSEE, or FPN) at a variety of incidence angles. These systems operated at K_u and K_a bands, 14 and 35 GHz, respectively. Only data from the K_u band system are used here. This system was identical to the X band system described by Plant *et al* (1994); a higher frequency oscillator had simply been substituted in the same system. The system used two antennas, one for transmitting and one for receiving. Both antennas were dual polarized, and the two polarizations were rendered separable upon reception by offsetting the transmitted frequencies by 60 MHz, horizontal polarization being the higher. Only like polarizations on transmission and reception, HH and VV, were recorded. One-way, half-power antenna beamwidths at the K_u band were 6.6° in the E-plane and 5.0° in the H-plane, and the antennas were operated at a height of 26 m above mean low water level for all measurements reported here. These numbers imply that the illuminated surface area varies from 15 m^2 at a 45° incidence angle to 308 m^2 at 75°.

Data were processed using analogue-to-digital and digital-signal-processing boards in a 386-based PC and recorded on write once/read many (WORM) optical disks. Data were sampled at 1575, 2100, or 3150 Hz/channel, separated into in-phase and quadrature channels for each polarization, collected into arrays of 512 samples each, and stored on the WORM disks. Thus the integration time for each sample of these time series was less than 0.6 ms, far shorter than the approximately 10 ms correlation times of the signals (Plant *et al* 1994). Calibrated cross sections were computed from these time series of received fields in subsequent processing. Calibration constants were determined both before and after the experiment. The equipment and calibration procedures used in collecting these data were identical to those described by Plant *et al* (1994); the reader is referred to that paper for more details.

We collected data by varying the incidence angle of the antennas over the range 45° to 85°. The antenna look direction was held fixed but since the wind direction changed, a variety of look directions relative to the wind direction were obtained. Record lengths at each incidence angle were between 17 and 146 s. Wind speed and direction were obtained using an anemometer operated by FPN personnel. The anemometer height was 41 m. The wind speeds reported here are those at 10 m height, obtained from a logarithmic profile by dividing the measured values by 1.12. Wind speeds at 10 m ranged from 5 to 17.5 m s^{-1} during data collection.

3. Simulations using standard Bragg/composite surface theory

The use of slightly different microwave frequencies for HH and VV in this experiment ensured that the transmitted signals at the two polarizations had completely random phases. This turns out to be a very fortuitous situation for simulating sea return. If the transmitted signals had been phase locked, then the degree of correlation in the return signals at different polarizations would have depended on the precise phase between the vertically and horizontally transmitted

signals and on the degree of overlap of the illuminated areas at VV and HH. These would then have affected the calculation of the probability that $\sigma_o(\mathrm{HH}) > \sigma_o(\mathrm{VV})$, which we denote $\mathrm{P}(\sigma_o(\mathrm{HH}) > \sigma_o(\mathrm{VV}))$. For transmission having random phases between the polarizations, these effects do not matter since they only add further phase decorrelation to fields that are already phase decorrelated.

Thus we modelled return from the sea surface using a Monte Carlo simulation of Bragg/composite surface theory in which the fields received from different facets were assumed have independent random phases for horizontal and vertical polarizations. In total 100 random samples of sea surface slope were drawn from a population that had a variance equal to the difference between the variances measured by Cox and Munk (1954) for a clean surface and a slick-covered surface. These were assumed to be the tilts due to waves of intermediate scales of 100 different facets selected from all the facets within the sea-surface area illuminated by the antenna (Plant 2002). While this is not strictly true because very short waves contribute to Cox and Munk's clean-surface variances, the amount by which the variances should be reduced to exclude effects of very short waves is uncertain and we found it to make little difference in our simulations. The number of samples used here is somewhat arbitrary but if the 100 facets are selected uniformly from the total set of facets that cover the illuminated area, then the implied spacing between facets in each direction is 0.39 m at a 45° incidence angle and 1.75 m at 75°. Plant *et al* (1994) found that decorrelation lengths for sea return at both X and the K_a band were about 10 times the microwave length. Applying this to the K_u band implies that the decorrelation length, or facet dimension, is about 0.21 m, so the fields scattered by our 100 selected facets are well decorrelated.

This procedure was applied to both upwind and cross wind slopes. Negative slopes indicate that the surface normal tilts in the wind direction for upwind slopes; cross wind slopes are positive to the right of the wind direction. To these 100 intermediate-scale slope samples, a single sample of long-wave slope was added. The population from which the long-wave slope was drawn had variances in upwind and cross wind directions given by Cox and Munk's (1954) data for slick-covered surfaces. The slopes obtained from this procedure were rotated by the angle between the direction from which the wind came and the horizontal antenna look direction, χ, to yield slopes s_x in the plane of incidence and s_y perpendicular to it. The local incidence angle θ' in radians was then given by

$$\theta' = \theta + \tan^{-1} s_x \tag{1}$$

where θ is the nominal incidence angle. If θ' became less than 20°, it was set to 20°. This occurred less than 10% of the time at our highest wind speeds. If θ' became greater than 90°, it was set to 90°. This occurred a maximum of 15% of the time at incidence angles of 75°, 30% of the time at 80°, and 50% of the time at 85°.

Bragg wave spectral densities were taken to be

$$F(k_\mathrm{b}) = B/k_\mathrm{b}^4 \tag{2}$$

where k_b is the Bragg wavenumber given by

$$k_\mathrm{b} = 2k_o \sin\theta' \tag{3}$$

where k_o is the microwave number. Since the object of this exercise was not to determine short wave spectral densities, we let B have a value that at each wind speed provided the best fit to measured values of $\sigma_o(\mathrm{VV})$ at all incidence angles. These fits showed that B was given approximately by $B = 0.001 + 0.000\,06U$ where U is wind speed in m s^{-1}.

We then calculated the fields received from the jth facet of the 100 selected facets according to

$$E_{\mathrm{h}j} = g'_{\mathrm{hh}}\sqrt{16\pi k_o^4 F(k_\mathrm{b})}\,\mathrm{e}^{\mathrm{i}\alpha_{\mathrm{h}j}} \tag{4}$$

$$E_{vj} = g_{vv}\sqrt{16\pi k_o^4 F(k_b)}\,e^{i\alpha_{vj}} \tag{5}$$

where α_{hj} and α_{vj} are independent random phases for HH and VV drawn from a population uniformly distributed between 0 and 2π. The geometric coefficients g'_{hh} and g_{vv} are given by (Plant 1990)

$$g_{vv} = (\epsilon - 1)(\epsilon(1 + \sin^2\theta') - \sin^2\theta')\cos^2\theta' \Big/ \left(\epsilon\cos\theta' + \sqrt{\epsilon - \sin^2\theta'}\right)^2 \tag{6}$$

$$g_{hh} = (\epsilon - 1)\cos^2\theta' \Big/ \left(\cos\theta' + \sqrt{\epsilon - \sin^2\theta'}\right)^2 \tag{7}$$

$$g'_{hh} = \cos^2\phi\, g_{hh} + \sin^2\phi\, g_{vv} \tag{8}$$

where ϵ is the dielectric constant of water and ϕ is the tilt out of the plane of incidence given by

$$\phi = \tan^{-1}(\tan^{-1} s_y/\theta'). \tag{9}$$

In order to include fading in the calculations, the fields from the 100 facets were added together and the magnitude of the sum was squared and divided by 100 to get σ_o(VV) and σ_o(HH):

$$\sigma_o(\mathrm{VV}) = |\Sigma_{j=0}^{100} E_{vj}|^2/100 \tag{10}$$

$$\sigma_o(\mathrm{HH}) = |\Sigma_{j=0}^{100} E_{hj}|^2/100. \tag{11}$$

This yields a single realization of each σ_o(VV) and σ_o(HH). This procedure was repeated ten thousand times and averaged to produce the mean values $\langle\sigma_o(\mathrm{VV})\rangle$ and $\langle\sigma_o(\mathrm{HH})\rangle$ and therefore the mean polarization ratio, $\langle\sigma_o(\mathrm{HH})\rangle/\langle\sigma_o(\mathrm{VV})\rangle$. From the array of realizations, we calculated P(σ_o(HH) $>$ σ_o(VV)), the probability density function (PDF) of the polarization ratio, P(σ_o(HH)/σ_o(VV)), the probability of a particular scattering amplitude (square root of cross section) and the correlation coefficient between the cross sections σ_o(VV) and σ_o(HH).

The same quantities can readily be computed from the measured sea return at HH and VV polarizations. Figure 1 shows the results obtained from the measurements and simulations for one time series measured at $\theta = 45°$, $\chi = 5°$, and a wind speed of 8.5 m s^{-1}. Simulation using Bragg/composite surface theory clearly agrees rather well with measurements at this incidence angle, both yielding appreciable values of P(σ_o(HH) $>$ σ_o(VV)). Table 1 gives values of σ_o(HH) and σ_o(VV) measured and simulated (data and standard simulations). If we define the amplitude a of the backscatter to be the square root of the cross section, we may also compare simulations and measurements of PDFs of a/a_o and a where a_o is the square root of the mean cross section. Figure 2 shows such PDFs for the conditions of the same data set that was used to produce figure 1. Note that the obvious floor under the simulated distributions in figure 2(b) is due to the limited number of realizations and the logarithmic scale. It is impossible for a bin to contain a value less than 1 and stay on the logarithmic scale. Since our bin width, $\Delta(a/a_o)$ is 0.05, the minimum probability density that can be displayed is $1/(0.05 \times 10\,000)$, or 2×10^{-3}. These distributions are not Rayleigh, in agreement with Gotwols and Thompson (1994). Also in agreement with Gotwols and Thompson, we have found that our simulated distributions become Rayleigh if no tilting by long waves is included.

We have produced figures such as figures 1 and 2 for all wind speeds and azimuth angles for which we have data from SAXON-FPN, a total of 64 runs. We have found that the good simulation of the data obtained at 45° cannot be reproduced at higher incidence angles by this standard Bragg/composite surface theory. Examples are shown in figures 3 and 4 for $\theta = 75°$, $\chi = -10°$, and a wind speed of 7.6 m s^{-1}; again cross section values are given in table 1. Clearly the low values of σ_o(HH) predicted by Bragg/composite surface theory are incorrect.

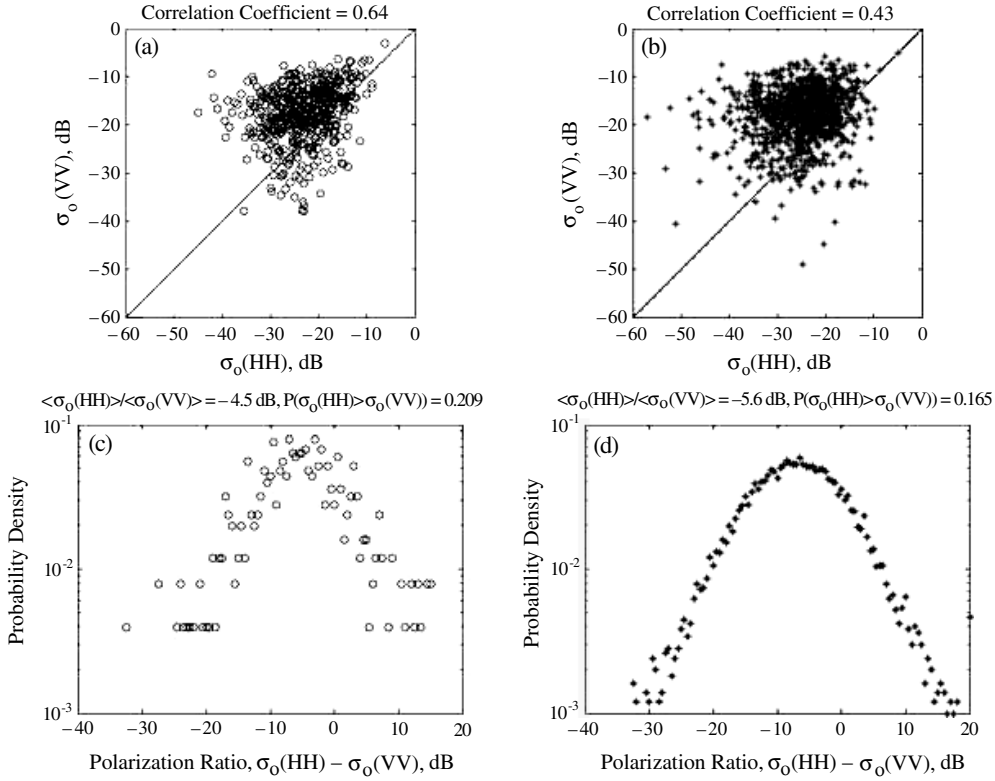

Figure 1. Distributions of cross sections and polarization ratios at $\theta = 45°$, $\chi = 5°$, and a wind speed of 8.5 m s^{-1}. (a) Scatter plot of measured σ_o(VV) versus σ_o(HH). (b) Scatter plot of σ_o(VV) versus σ_o(HH) simulated using Bragg/composite surface theory. (c) PDF of measured polarization ratios. (d) PDF of simulated polarization ratios.

Table 1. Measured and simulated cross sections. The wind speed was 8.5 m s^{-1} at $\theta = 45°$ and 7.6 m s^{-1} at $\theta = 75°$.

Type of cross section (dB)	$\theta = 45°$	$\theta = 75°$
$\langle\sigma_o(\mathrm{VV})\rangle$ data	−14.9	−22.7
$\langle\sigma_o(\mathrm{VV})\rangle$ standard simulations	−15.1	−23.6
$\langle\sigma_o(\mathrm{VV})\rangle$ bound wave simulations	−13.9	−22.4
$\langle\sigma_o(\mathrm{VV})\rangle$ full simulations	−14.6	−22.7
$\langle\sigma_o(\mathrm{HH})\rangle$ data	−19.4	−31.4
$\langle\sigma_o(\mathrm{HH})\rangle$ standard simulations	−20.9	−40.9
$\langle\sigma_o(\mathrm{HH})\rangle$ bound wave simulations	−18.5	−36.4
$\langle\sigma_o(\mathrm{HH})\rangle$ full simulations	−18.9	−31.9

4. Simulations including bound waves

Plant (1997) showed that bound, tilted waves generated by longer waves and travelling with these longer waves could account for the different behaviour of HH and VV microwave Doppler spectra at high incidence angles. The existence of such waves both in wind wave tanks and on the ocean has been clearly established (Duncan *et al* 1994, Hara *et al* 1997, Duncan *et al* 1999, Plant *et al* 1999b, 1999a, 1999c, Plant 2003). It is convenient to refer to the short waves of the

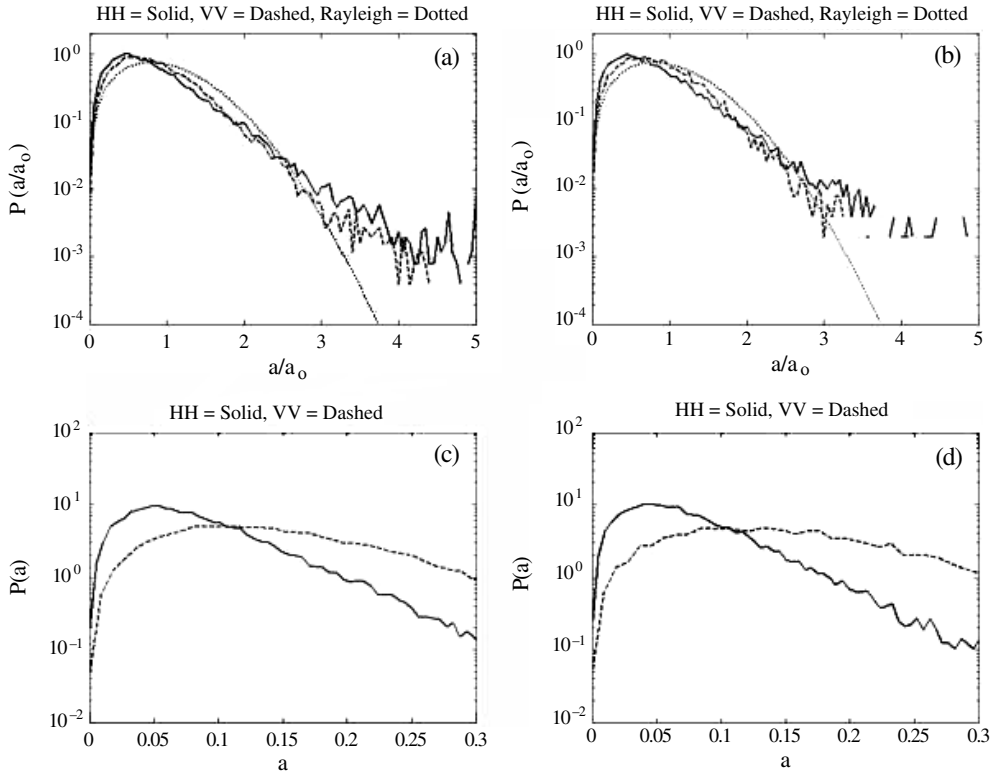

Figure 2. Probability distributions of backscattered amplitude at $\theta = 45°$, $\chi = 5°$, and a wind speed of 8.5 m s^{-1}. (a) PDF of a/a_o for measured HH and VV returns and for a Rayleigh distribution. (b) PDF of a/a_o for HH and VV returns simulated using Bragg/composite surface theory. (c) PDF of a for measured sea return. (d) PDF of a for simulated sea return.

previous section as free waves since they are not bound to any longer waves and propagate at their intrinsic phase speed.

We can add bound waves to the simulations described in the previous section. The changes necessary to apply the same procedure to bound waves as we did to free waves is to add the mean slope of the bound waves, $\langle s_b \rangle$, to the upwind slopes, to substitute the bound wave variance, σ_b^2, for upwind variance, to set the cross wind variance to zero and to change the degree of saturation B to

$$B_b = f(s_u) k_b B \tag{12}$$

where s_u is the tilt of the facet in the upwind direction caused by intermediate-scale waves and k_b is evaluated at the local incidence angle of the bound waves. This form for the bound wave degree of saturation, B_b, agrees with that found by Plant (1997) if $f(s)$ is constant. However, parameters for the bound waves must agree with those determined by Plant (2003) (see figure 5) from Cox and Munk (1954) sea-surface slope PDFs. The values of $\langle s_b \rangle$ found in this 2003 study are somewhat lower than those found to be necessary to account for high-incidence angle Doppler spectra (Plant 1997). Therefore, we have made the assumption here that the degree of saturation of the bound waves increases with the steepness of their parent waves and have taken

$$f(s_u) = 0.75\left[4\sqrt{(\sigma_b^2 - \sigma_s^2)} - s_u\right]^2 \tag{13}$$

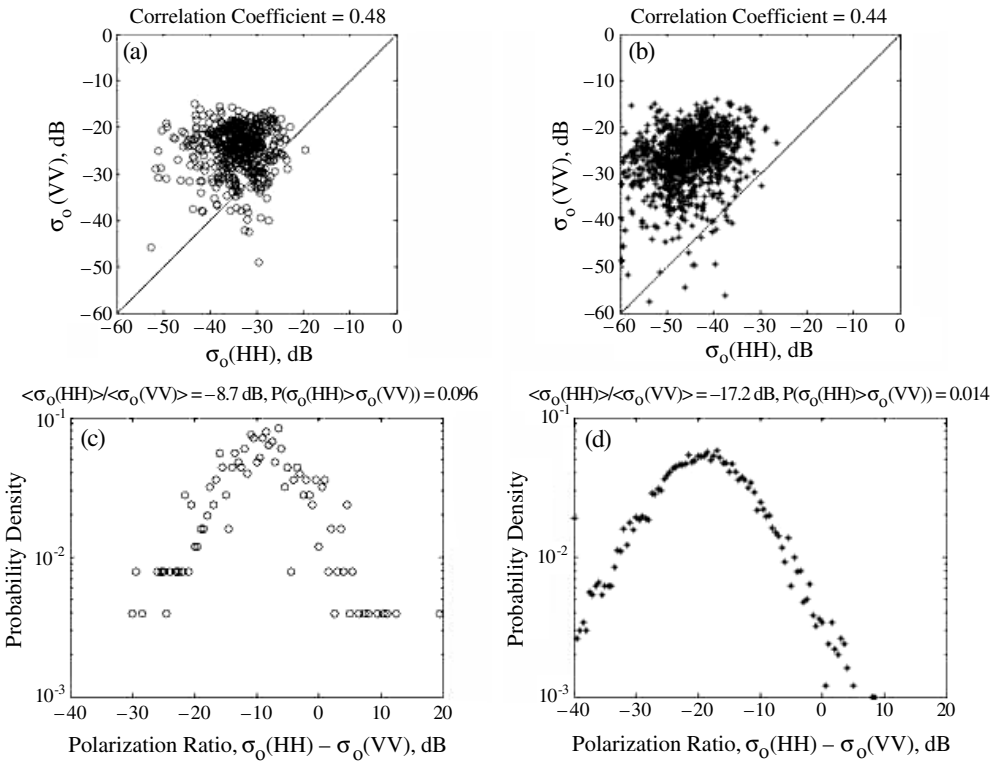

Figure 3. Same as figure 1 but for $\theta = 75°$, $\chi = -10°$ and a wind speed of 7.6 m s^{-1}.

where σ_s^2 is the slope variance of Cox and Munk's slick-covered surface. If the quantity in brackets becomes negative, $f(s_u)$ is set to zero. This form for $f(s_u)$ is small if the facet tilt is less than the mean bound wave slope and increases as the facet tilt becomes more negative, i.e. becomes more downwind than the mean bound wave slope. This procedure yields bound wave effects on the cross section that are in agreement with those of Plant (1997) but mean spectral densities of the bound waves now depend on their slope. Also, the lower mean bound wave slopes require that the spectral densities of the bound waves are somewhat higher than those determined by Plant (1997).

In addition to these bound wave changes, some modification of our treatment of free waves is necessary to include bound wave effects. Since the mean slope of the sea surface is zero, free waves must have a small mean tilt in the opposite direction to bound waves. This must be added to the upwind slopes in the free wave simulation. Similarly, free wave variances in the upwind direction are changed slightly by the existence of bound waves. Values of both the mean and variance of free wave slopes have been deduced from sea-surface probability distributions by Plant (2003); they are also shown in figure 5.

When E_h and E_v for bound waves have been computed according to this procedure, they are substituted for a fraction of the 100 field values at each polarization that is equal to the probability of finding bound waves according to Plant (2003) (see figure 5). Figure 6 shows the results at 45° incidence for the same conditions as shown in figures 1 and 2; mean cross sections are given in table 1 (bound wave simulations). Although the changes are small, the agreement with data is improved by the addition of bound waves. Figure 7 shows results

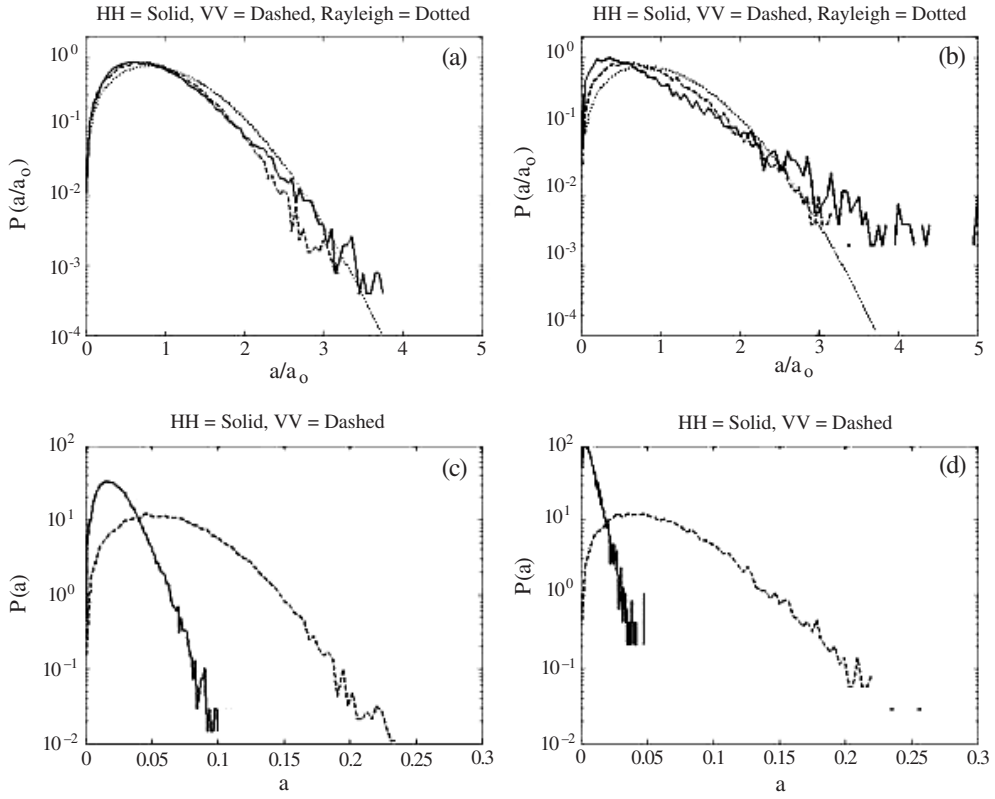

Figure 4. Same as figure 2 but for $\theta = 75°$, $\chi = -10°$ and a wind speed of 7.6 m s^{-1}.

of simulations at $\theta = 75°$ including bound waves for conditions of the same run shown in figures 3 and 4. The bound waves have increased the polarization ratio toward the larger values found experimentally but have not brought them into agreement. Cross sections $\langle\sigma_o(\mathrm{VV})\rangle$ and $\langle\sigma_o(\mathrm{HH})\rangle$ are again shown in table 1. Limits exist on the amount by which $\sigma_o(\mathrm{HH})$ and polarization ratios can be raised by bound waves. First, bound wave spectral densities cannot be made so large that their effects are significant at either polarization at 45° since data on the ocean do not support this. Furthermore, bound waves cannot affect $\sigma_o(\mathrm{VV})$ significantly at any incidence angle since ocean data again show that this is not the case. Finally, even if bound waves completely overwhelmed free, wind-generated, short waves, the polarization ratio could not be increased to more than that at a mean incidence angle of $\theta + \langle s_\mathrm{b}\rangle$ (recall that $\langle s_\mathrm{b}\rangle$ is negative). Thus bound waves do not appear to explain completely the problem that Bragg/composite surface theory predicts $\sigma_o(\mathrm{HH})$ values, and therefore polarization ratios, that are too low at high incidence angles.

5. Simulations including non-Bragg scattering

Insight into the nature of the under-prediction of $\sigma_o(\mathrm{HH})$ by Bragg scattering can be gained by plotting measured and simulated (including bound waves) mean cross sections versus incidence angle at various wind speeds. In figures 8(a) and (b), we show the dependence of $\langle\sigma_o(\mathrm{VV})\rangle$ and $\langle\sigma_o(\mathrm{HH})\rangle$ on incidence angle for wind speeds between 6 and 8 m s^{-1} and between 12

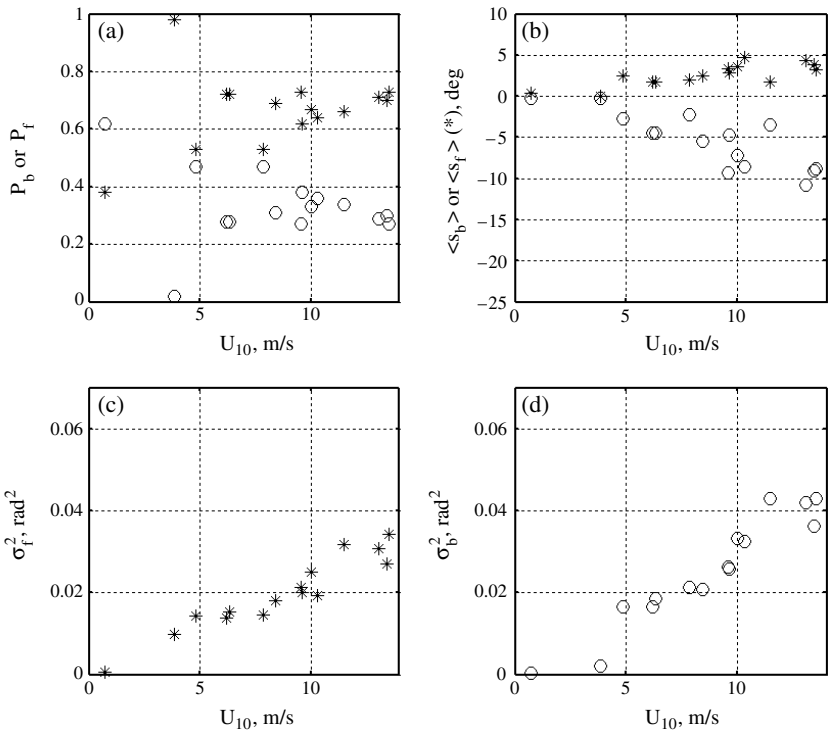

Figure 5. Bound and free wave parameters on the ocean versus wind speed at 10 m height (from Plant 2003). (a) Total probability of finding bound waves P_b (open circles) or free waves P_f (asterisks). (b) Mean slopes of bound waves $\langle s_\mathrm{b}\rangle$ (circles) or free waves $\langle s_\mathrm{f}\rangle$ (asterisks). (c) Variances of free wave slopes, σ_f^2. (d) Variances of bound wave slopes, σ_b^2.

and 14 m s^{-1}. Simulated values of $\langle\sigma_o(\mathrm{HH})\rangle$ fall increasingly below the measured values with increasing incidence angles. Furthermore, the measured values seem to become nearly constant at high incidence angles at levels that increase with wind speed. While we have adjusted B to produce the best wind speed dependence for $\langle\sigma_o(\mathrm{VV})\rangle$, its agreement with data as a function of incidence angle in figure 8(a) shows that Bragg scattering works very well for this polarization. In figures 8(c) and (d), we show the result of adding, in antilog space, a small additional cross section to the simulated values. The levels of cross section added to the simulated ones are $\Delta\sigma_o = -33$ dB at a wind speed of 7 m s^{-1} and $\Delta\sigma_o = -30$ dB at 13 m s^{-1}; they are constant with incidence angle and polarization. Figures 8(c) and (d) show that these small additional cross sections hardly affect $\langle\sigma_o(\mathrm{VV})\rangle$ at any incidence angle but that they bring high-incidence angle $\langle\sigma_o(\mathrm{HH})\rangle$ values up into agreement with measurements at incidence angles above 60° to 65°.

If we assume that the fields produced by this additional scattering are Gaussian distributed, then we may simulate their effect on $\mathrm{P}(\sigma_o(\mathrm{HH}) > \sigma_o(\mathrm{VV}))$ and $P(a)$ by adding the following fields to those derived from Bragg scattering:

$$E_\mathrm{s} = \sqrt{10^{\Delta\sigma_o/10}}\mathrm{e}^{\mathrm{i}\alpha_\mathrm{s}} \tag{14}$$

where α_s is uniformly distributed between 0 and 2π. Adding E_s to our simulations at 75° produces the results shown in figure 9. These are now in good agreement with data (see figures 3 and 4).

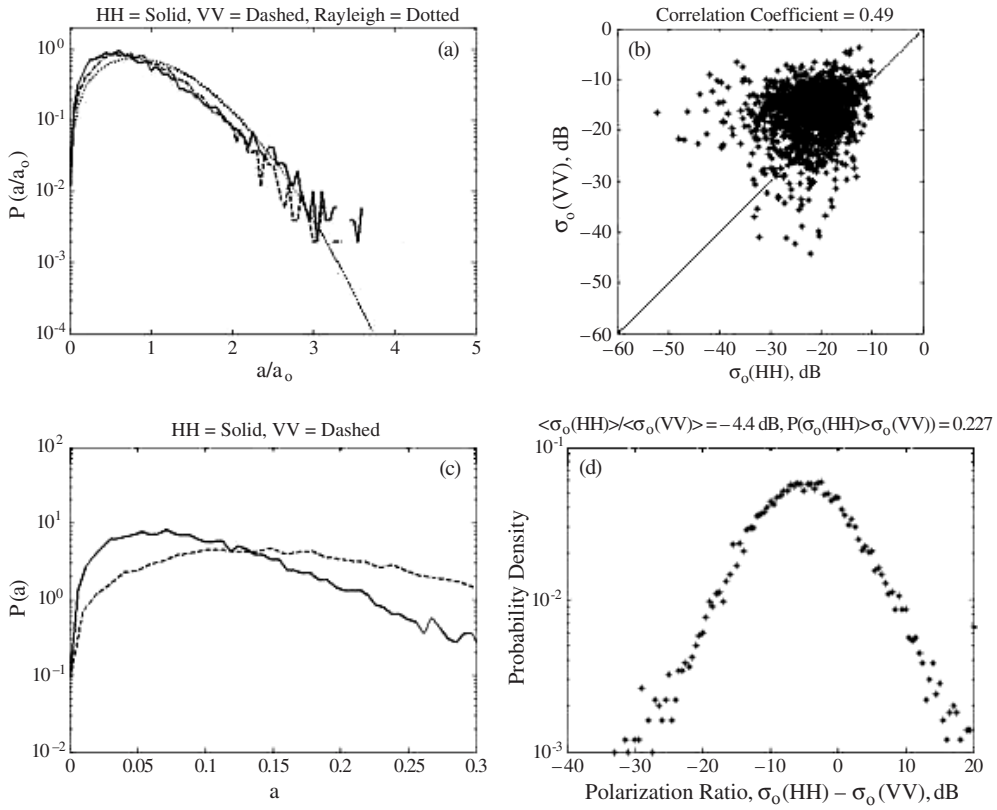

Figure 6. Simulations at $\theta = 45°$ including bound waves for the same run as shown in figures 1 and 2.

The addition of E_s also produces better agreement between data and simulations for the dependence of $P(\sigma_o(HH) > \sigma_o(VV))$ on the integration time. This is shown in figure 10 where 10(a) shows measurements and Bragg-only simulations of this dependence at 45° and 75°. In order to convert the averages over N decorrelated samples in the simulations to integration times, we have assumed that the correlation time can be deduced from Plant *et al* (1994), where it was found to depend on the illuminated area. Plant *et al* give correlation times at only 10 and 35 GHz. We have assumed that those at 14 GHz are 90% of those at 10 GHz. The agreement between simulations and data in figure 10(a) is rather good at 45°, showing that Bragg scattering dominates at this incidence angle. At 75°, however, simulated values of $P(\sigma_o(HH) > \sigma_o(VV))$ are much too low and fall with integration time differently than the data. Figure 10(b) shows the result of adding E_s to the simulations. Now data agree with simulations much better at 75°.

One possibility for the origin of this non-Bragg backscattering from the sea is spray close to the surface. If spherical, the spray droplets would scatter both polarizations equally. If not too dense, attenuation would be minimal and we show below that the scatter would be independent of incidence angle. As long as this scatter is small compared to surface scatter, as it is at VV polarization, spray would have little effect. As the mean surface scattering dropped to low values, as it does at HH polarization and high incidence angles, effects of the spray would begin to be noticable. The symmetry between this situation and that of acoustic

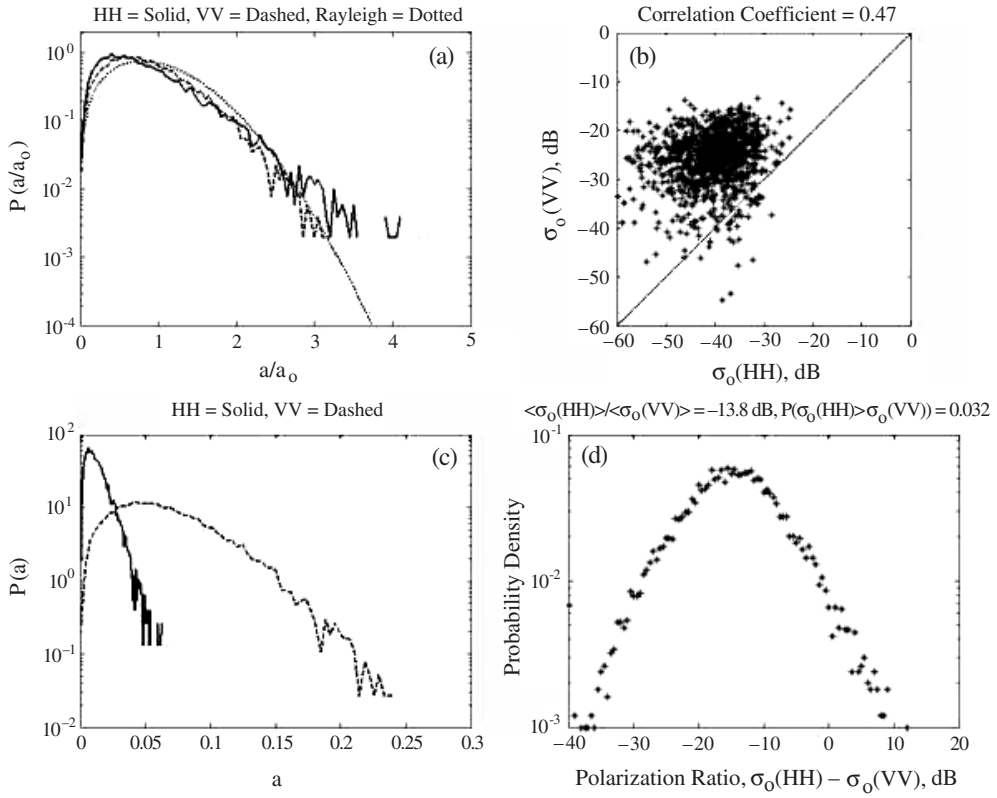

Figure 7. Simulations at $\theta = 75°$ including bound waves for the same run as shown in figures 3 and 4.

surface scattering adds to its feasibility. Acoustic surface scattering results from both the rough surface and bubbles near the surface (Dahl *et al* 1997). The difference may only be that bubbles dominate acoustic scattering at all but the lowest wind speeds because of their high concentrations while spray droplets, due to their low concentrations, make themselves known in microwave surface scatter only when rough surface scattering drops very low.

We can easily see if spray can yield extra cross sections that are consistent with those found above. Perfectly conducting spherical droplets will have cross sections given by

$$\sigma_s = \frac{\pi^5 D^6}{4\lambda^4} \tag{15}$$

if their diameter D is much smaller than the microwave length λ. This will transition to

$$\sigma_s = \frac{\pi D^2}{4} \tag{16}$$

or just the droplet cross section for very large droplets. The normalized radar cross section for spray droplets, $\sigma_o(S)$, will then be given by

$$\sigma_o(S) = \frac{6V}{A} \int \sigma_s \frac{\mathrm{d}N}{\mathrm{d}D}\,\mathrm{d}D \tag{17}$$

where $\frac{\mathrm{d}N}{\mathrm{d}D}$ is the number of droplets per unit volume per unit diameter, or the drop size

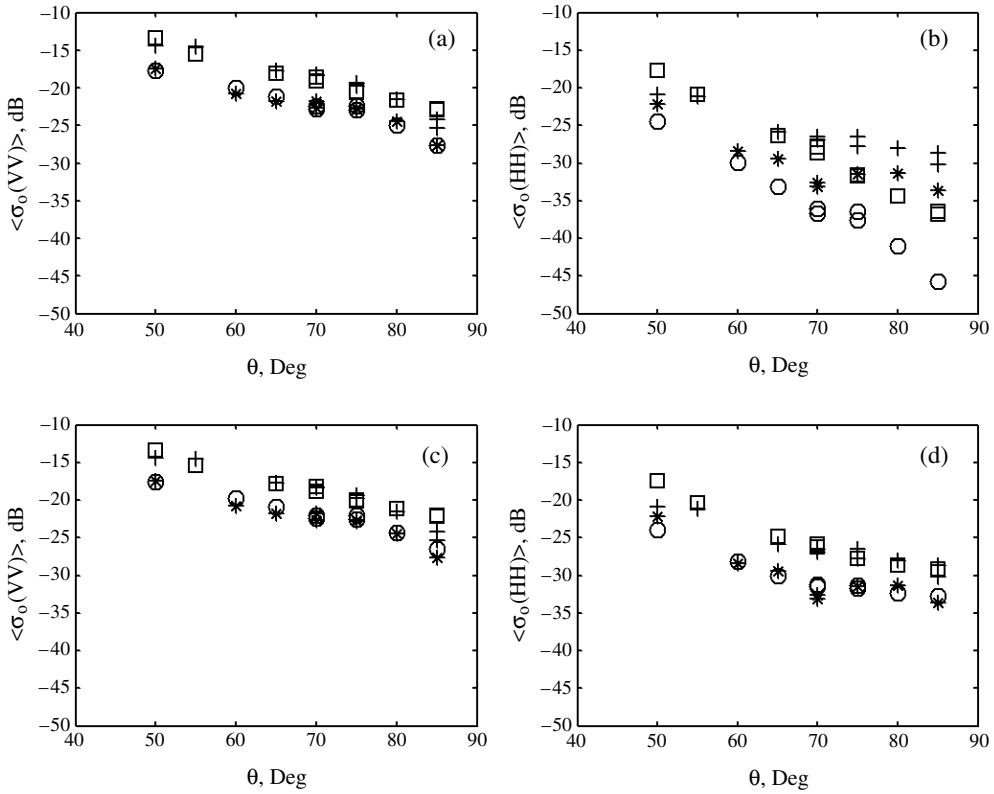

Figure 8. Measured and simulated mean cross sections versus incidence angle. Wind speed 6–8 m s^{-1}: asterisks = measured, circles = simulated; wind speed 12–14 m s^{-1}: pluses = measured, squares = simulated. (a) $\langle\sigma_o(\mathrm{VV})\rangle$ versus θ; (b) $\langle\sigma_o(\mathrm{HH})\rangle$ versus θ; (c) $\langle\sigma_o(\mathrm{VV})\rangle$ versus θ with $10^{\Delta\sigma_o/10}$ added to the simulated $\sigma_o(\mathrm{VV})$; (d) $\langle\sigma_o(\mathrm{HH})\rangle$ versus θ with $10^{\Delta\sigma_o/10}$ added to the simulated $\sigma_o(\mathrm{HH})$. All simulations are for Bragg scattering from free and bound waves. $\Delta\sigma_o = -33$ dB at a wind speed of 7 m s^{-1} and -30 dB at 13 m s^{-1}.

distribution, V is the illuminated volume and A is the illuminated area given by

$$A = \frac{\pi}{4}\Phi_\mathrm{h}\Phi_\mathrm{v}H^2/\cos^3\theta \tag{18}$$

where Φ_h and Φ_v are horizontal and vertical one-way, full, half-power antenna beamwidths in radians and H is the height of the antenna above the mean water level. Then the volume V illuminated up to a height $z = 1$ m above the mean water level by a pencil-beam antenna can easily be calculated from

$$V = \int_0^1 A(H-z)^2/H^2\,\mathrm{d}z = A\left(1 - \frac{2}{H} + \frac{1}{3H^2}\right). \tag{19}$$

The factor of 6 in (17) is due to reflection of the incident radiation from the sea surface combined with scattering from droplets in addition to direct backscatter from the droplets.

Wavetank measurements of spray droplets above a wind-roughened water surface show that $\frac{\mathrm{d}N}{\mathrm{d}D}$ goes as D^{-3} and U^5, where U is the wind speed, for droplet diameters up to 1.5 mm, the limit of the instrument used (Chris Fairall, private conversation). We have used $\frac{\mathrm{d}N}{\mathrm{d}D}$ with this dependence on D to simulate expected values of $\sigma_o(S)$. We found that the wind speed dependence had to be reduced to U^1 in order to yield $\Delta\sigma_o$ values in agreement with our

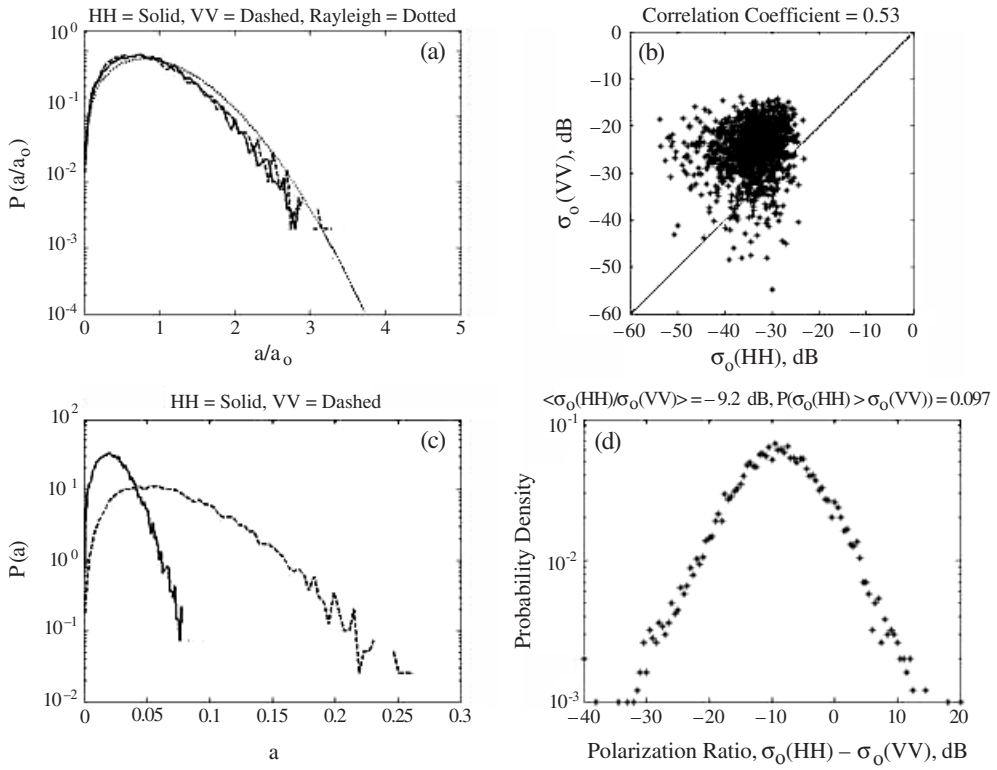

Figure 9. Simulations at $\theta = 75°$ with an added Gaussian field of magnitude $\sqrt{10^{\Delta\sigma_o/10}}$. These simulations are for the same run as figures 3, 4 and 7.

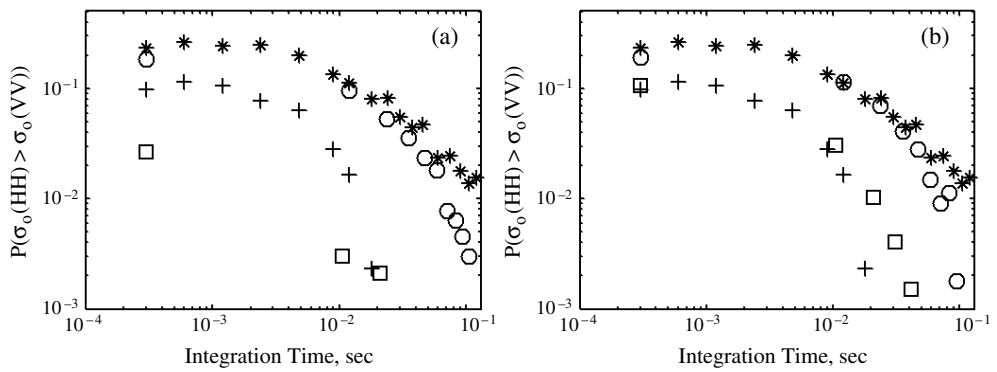

Figure 10. The dependence of P(σ_o(HH) > σ_o(VV)) on integration time. (a) Measurements compared with Bragg simulations, (b) measurements compared with simulations adding E_s. Symbols represent the following: circles—$\theta = 45°$, simulated; asterisks—$\theta = 45°$, measured; squares—$\theta = 75°$; pluses—$\theta = 75°$, measured.

measurements. When this was done, however, the results were quite encouraging, as shown in figure 11. Droplets smaller than about 1 mm had very little effect on the backscatter. However, droplets larger than 1 cm still contributed and, if present, would increase the cross

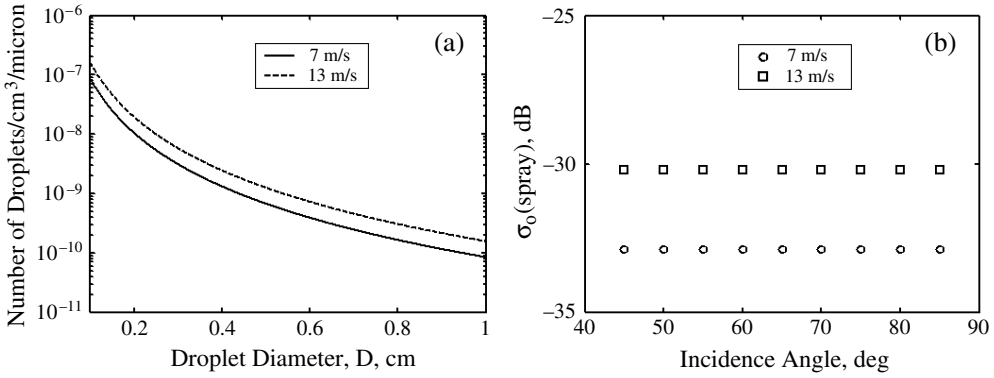

Figure 11. (a) Assumed distribution of spray droplets, and (b) their resulting normalized radar cross section versus incidence angle at two different wind speeds.

section somewhat. We simulated $\sigma_o(S)$ by assuming that large drops become less probable than given by our drop size distribution and we cut off the distribution at 1 cm. Under these conditions, the volume V would contain about 60 droplets (4 droplets m^{-3}) on average at 45° incidence and a wind speed of 7 m s^{-1}. This is sufficient to ensure that E_s is Gaussian. Clearly the levels of $\sigma_o(S)$ shown in figure 11(b) agree very well with our measured $\Delta\sigma_o$. Furthermore, they show no dependence on incidence angle or polarization. Before this is considered to be a valid explanation of the observed non-Bragg backscatter, however, we must await more conclusive measurements of the characteristics of droplet distributions just above the sea surface.

6. Discussion and conclusion

We have not included hydrodynamic modulation of free waves in the simulations. One reason is that this formulation is difficult to apply to the probabilistic approach taken here. Other reasons are that for many of our incidence angles tilt dominates hydrodynamic modulation, and that hydrodynamic modulation is generally small at the wind speeds in our data set. It could also be, though, that much of the modulation attributed to freely propagating short wind waves is in reality due to the modulation of intermediate-scale waves that then generate bound short waves. The modulation of the intermediate waves would be represented here by the mean tilt of the bound waves. In order for this idea to explain past measurements of modulation transfer functions, intermediate waves would have to be advected by larger waves and their phase speeds would have to be less than the sub-footprint velocity fluctuations in typical measurements.

Even without hydrodynamic modulation, our simulations have demonstrated that Bragg scattering predicts that σ_o(HH) can be greater than σ_o(VV) as much as 25% of the time in the mid-range of incidence angles if the integration time does not exceed the correlation time. This agrees with experiment. Bragg scattering predictions of the probability that σ_o(HH) exceeds σ_o(VV) and of the probability distributions of scattering amplitude are also in good agreement with data in the mid-range of incidence angles, especially if Bragg scattering from bound waves is included in the simulations. At higher incidence angles the agreement deteriorates due to the under-prediction of σ_o(HH) by Bragg/composite scattering theory, even with bound waves included. The situation can be rectified if a small, non-Bragg component of backscatter is

added to the Bragg/composite predictions. This small, additional, cross section is independent of polarization and incidence angle but depends on wind speed. One possible explanation for this additional backscatter is scattering from spray droplets above the sea surface.

Acknowledgments

This work was supported by the Office of Naval Research Space and Remote Sensing Programme under grants number N00014-00-1-0075 and N00014-01-1-0153.

References

Bass F G, Fuks I M, Kalmykov A I, Ostrovsky I E and Rosenberg A D 1968 Very high frequency radiowave scattering by a disturbed sea surface. Part II: scattering from an actual sea surface *IEEE Trans. Antennas Propag.* **16** 560–8

Cox C and Munk W 1954 Statistics of the sea surface derived from sun glitter *J. Mater. Res.* **13** 199–227

Dahl P H, Plant W J, Nützel B, Schmidt A, Herwig H and Terray E A 1997 Simultaneous acoustic and microwave backscattering from the sea surface *J. Acoust. Soc. Am.* **101** 2583–95

Donelan M A and Pierson W J Jr 1987 Radar scattering and equilibrium ranges in wind-generated waves with application to scatterometry *J. Geophys. Res.* **92** 4971–5029

Duncan J H, Philomin V, Behres M and Kimmel J 1994 The formation of spilling breaking water waves *Phys. Fluids* **6** 2558–60

Duncan J H, Qiao H, Philomin V and Wenz A 1999 Gentle spilling breakers: crest profile evolution *J. Fluid Mech.* **379** 191–222

Gotwols B L and Thompson D R 1994 Ocean microwave backscatter distributions *J. Geophys. Res.* **99** 9741–50

Hara T, Bock E J and Donelan M 1997 Frequency-wavenumber spectrum of wind-generated gravity-capillary waves *J. Geophys. Res.* **102** 1061–72

Kwoh D S W, Lake B M and Rungaldier H 1988 Microwave scattering from internal wave modulated surface waves: a shipboard real aperture coherent radar study in the Georgia Strait Experiment *J. Geophys. Res.* **93** 12235–49

Lee P H Y, Barter J D, Beach K L, Hindman C L, Lake B M, Rundaldier H, Shelton J C, Williams A B, Yee R and Yuen H C 1995 X-band microwave backscattering from ocean waves *J. Geophys. Res.* **100** 2591–611

Lee P H Y, Barter J D, Beach K L, Hindman C L, Lake B M, Rundaldier H, Thompson H R and Yee R 1997 Experiments on Bragg and non-Bragg scattering using single-frequency and chirped radars *Radio Sci.* **32** 1725–44

Lee P H Y, Barter J D, Beach K L, Lake B M, Rundaldier H, Thompson H R Jr, Wang L and Yee R 1999 What are the mechanisms for non-Bragg scattering from water wave surfaces? *Radio Sci.* **34** 123–38

Lyzenga D R, Maffett A L and Shuchman R A 1983 The contribution of wedge scattering to the radar cross section of the ocean surface *IEEE Trans. Geosci. Remote Sens.* **21** 502–5

Plant W J 1990 Bragg scattering of electromagnetic waves from the air/sea interface *Surface Waves and Fluxes: Current Theory and Remote Sensing* vol 2, ed G L Geernaert and W J Plant (Dordrecht: Kluwer) pp 41–108

Plant W J 1997 A model for microwave Doppler sea return at high incidence angles: Bragg scattering from bound, tilted waves *J. Geophys. Res.* **102** 21131–46

Plant W J 2002 A stochastic, multiscale model of microwave backscatter from the ocean *J. Geophys. Res.* **107** 3120 doi:10.1029/2001JC000909

Plant W J 2003 A new interpretation of sea-surface slope probability density functions *J. Geophys. Res.* at press

Plant W J and Alpers W 1994 An introduction to SAXON-FPN *J. Geophys. Res.* **99** 9699–703

Plant W J, Dahl P H and Keller W C 1999a Microwave and acoustic scattering from parasitic capillary waves *J. Geophys. Res.* **104** 25853–66

Plant W J, Keller W C, Hesany V, Hara T, Bock E and Donelan M 1999b Bound waves and Bragg scattering in a wind wavetank *J. Geophys. Res.* **104** 3243–63

Plant W J, Keller W C, Hesany V, Hayes K, Dahl P, Hara T, Bock E and Donelan M 1999c 'Crumpling' wave effects in backscatter from the air-sea interface *The Wind-Driven Air-Sea Interface* ed M L Banner (Canberra, Australia: ADFA Document Production Centre) pp 409–16

Plant W J, Keller W C, Petitt R A and Terray E A 1994 The dependence of microwave backscatter from the sea on illuminated area: correlation times and lengths *J. Geophys. Res.* **99** 9705–23

Rufatt L M 1999 Radar backscatter from the ocean surface *PhD Thesis* University of Sydney

Walker D 2000 Experimentally motivated model for low grazing angle radar Doppler spectra of the sea surface *IEE Proc., Radar Sonar Navig.* **147** 114–20

Wright J W 1968 A new model for sea clutter *IEEE Trans. Antennas Propag.* **16** 217–23